True Mechanism of Spontaneous Order from Turbulence in Two-Dimensional Superfluid Manifolds

Toshiaki Kanai[1,2] and Wei Guo[1,3,*]

[1]National High Magnetic Field Laboratory, 1800 East Paul Dirac Drive, Tallahassee, Florida 32310, USA
[2]Department of Physics, Florida State University, Tallahassee, Florida 32306, USA
[3]Mechanical Engineering Department, FAMU-FSU College of Engineering, Florida State University, Tallahassee, Florida 32310, USA

(Received 16 April 2021; accepted 30 July 2021; published 24 August 2021)

In a 2D turbulent fluid containing pointlike vortices, Lars Onsager predicted that adding energy to the fluid can lead to the formation of persistent clusters of like-signed vortices, i.e., Onsager vortex (OV) clusters. In the evolution of 2D superfluid turbulence in a uniform disk-shaped Bose-Einstein condensate (BEC), it was discovered that a pair of OV clusters with opposite signs can form without any energy input. This striking spontaneous order was explained as being due to a vortex evaporative-heating mechanism, i.e., annihilations of vortex-antivortex pairs which remove the lowest-energy vortices and thereby boost the mean energy per vortex. However, in our search for exotic OV states in a boundaryless 2D spherical BEC, we found that OV clusters never form despite the annihilations of vortex pairs. Our analysis reveals that contrary to the general belief, vortex-pair annihilation emits intense sound waves, which damp the motion of all vortices and hence suppress the formation of OV clusters. We also present unequivocal evidence showing that the true mechanism underlying the observed spontaneous OV state is the vortices exiting the BEC boundaries. Uncovering this mechanism paves the way for a comprehensive understanding of emergent vortex orders in 2D manifolds of superfluids driven far from equilibrium.

DOI: 10.1103/PhysRevLett.127.095301

In 2D turbulent flows such as in soap films [1] and Jupiter's atmosphere [2], large-scale persistent vortex structures are often observed. The appearance of these large-scale vortices can be understood in terms of a simplified point-vortex model proposed by Onsager [3]: when energy is continuously injected into a finite-sized 2D fluid containing many pointlike vortices, the like-signed vortices must eventually aggregate to form large clusters [i.e., Onsager vortex (OV) clusters] in order to sustain the high kinetic energy of the fluid. This ordered OV state is associated with a negative temperature since it has more energy but less entropy as compared to a state with randomly distributed vortices [3]. While Onsager's model has provided valuable insights into 2D turbulence in general [4,5], it is particularly relevant to 2D superfluids, such as planar Bose-Einstein condensates (BECs) [6,7] and superfluid helium films [8,9], where the vortices are indeed pointlike topological defects with a quantized circulation [10].

Surprisingly, recent numerical simulations of 2D turbulence in uniform disk-shaped BECs uncovered that a pair of OV clusters with opposite signs can form even in the absence of any energy input [11,12]. This intriguing spontaneous emergence of order from chaos has prompted extensive subsequent research [13–19]. A widely accepted explanation is that this emergent order is caused by a vortex evaporative-heating mechanism [11,12], i.e., annihilations of vortex-antivortex pairs at close separation. Such pairs of vortices induce negligible flows in the BEC. Therefore, their annihilations merely decrease the number of vortices but retain the total energy of the vortex system, which thereby increases the mean energy per vortex. For a disk-shaped BEC with a radius R carrying zero angular momentum but sufficient energy, it has been shown that as the vortices keep annihilating, the vortex system can evolve into the negative temperature state and eventually approach a limiting configuration consisting of two concentrated vortex clusters separated symmetrically around the disk center by about $0.922R$ [13], as shown in Fig. 1(a).

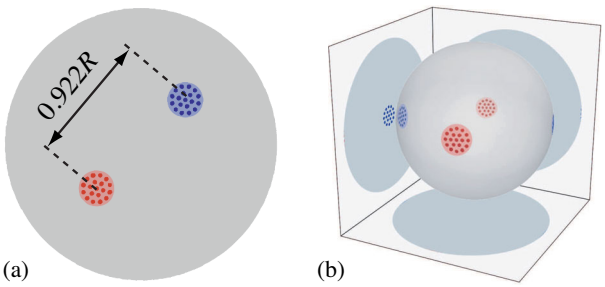

FIG. 1. Schematics showing the limiting configuration of OV clusters in 2D BECs with zero angular momentum in (a) planar disk geometry and (b) spherical shell geometry. The points of different colors represent vortices of different signs.

This limiting configuration gives the highest kinetic energy per vortex.

Recently, there has been increasing interest in BECs confined in a spherical shell geometry [20–24]. Creating such a curved BEC manifold using a spherical bubble trap was proposed two decades ago [25], but later research showed that this could be achieved only in microgravity since otherwise the atoms would fall to the bottom of the trap [26,27]. Nevertheless, this technical barrier was conquered recently due to the installation of the NASA cold atom laboratory at the International Space Station [28,29]. Unlike the disk BEC case, the formation of any dipole OV-cluster configuration in 2D turbulence on a spherical surface is always associated with a finite angular momentum and therefore is prohibited if the BEC has zero angular momentum to begin with. In this situation, a novel quadrupole limiting configuration with two pairs of like-signed OV clusters across two perpendicular diameters is expected [see Fig. 1(b)], since the corresponding flow field carries the highest kinetic energy with zero angular momentum.

In this Letter, we discuss our search for the exotic OV states in 2D spherical BECs. To our surprise, we find that OV clusters never form despite the annihilations of vortex pairs. We then present unequivocal analysis results to show that the spontaneous OV state in isolated BECs is not due to vortex-pair annihilations but instead is caused by vortices exiting the BEC boundaries. Uncovering this true mechanism not only explains the absence of OV clusters in boundaryless 2D spherical BECs but also advances our knowledge of spontaneous vortex orders in 2D superfluid manifolds in general.

Numerical method.—We model the dynamics of the BECs at low temperatures using the three-dimensional Gross-Pitaevskii equation (GPE) [30]:

$$i\hbar\frac{\partial\psi}{\partial t}=\left[-\frac{\hbar^2}{2m}\nabla^2+U(\mathbf{r},t)+g|\psi|^2\right]\psi, \tag{1}$$

where $\psi=|\psi|e^{i\phi}$ is the condensate wave function, m is the particle mass, g is the coupling constant, and U is the external potential that confines the BEC. To generate quasi-2D BECs in both the disk and the spherical shell geometries for comparative studies, we adopt the confining potential used in Ref. [11] to create a disk BEC:

$$U(\mathbf{r})=U_0\{\tan h[(r-R)/a_{\rm osc}]+1\}+\frac{1}{2}m\omega^2z^2, \tag{2}$$

where U_0 and ω are parameters pertinent to the trap strength in the radial plane and along the z axis. $a_{\rm osc}=\sqrt{\hbar/m\omega}$ is the characteristic trapping length in the z direction that controls the disk thickness, and R sets the disk radius. To create a spherical BEC shell, the following radial potential is used [20–22]:

$$U(\mathbf{r})=\frac{1}{2}m\omega^2(r-R)^2. \tag{3}$$

For convenience, we normalize the time and length scales as $\tilde{t}=\omega t$ and $\tilde{r}=r/a_{\rm osc}$ so the original GPE can be written in a dimensionless form:

$$i\frac{\partial\tilde{\Psi}}{\partial\tilde{t}}=\left[-\frac{1}{2}\tilde{\nabla}^2+\frac{U}{\hbar\omega}+\tilde{g}|\tilde{\Psi}|^2\right]\tilde{\Psi}, \tag{4}$$

where $\tilde{\psi}=\psi/(\sqrt{N/a_{\rm osc}^3})$ with $N=\int dV|\psi|^2$ being the total particle number. We select the trap parameters such that the normalized coupling constant $\tilde{g}=gN/\hbar\omega a_{\rm osc}^3=\sqrt{125}\times10^4$ and $U_0/\hbar\omega=64$, matching with those in Ref. [11] and the experimental work [31]. The radius for the disk BEC is set to $\tilde{R}=R/a_{\rm osc}=30$ and for the spherical BEC shell is $\tilde{R}=15$, so the two BECs have the same surface areas.

We then numerically imprint [22,32,33] the velocity field of 80 vortices and 80 antivortices at random locations in the two BECs while keeping their angular momentum nearly zero [11]. Equation (4) is evolved in imaginary time for a short period to heal the vortex-core structure [34]. The dynamical evolution of the condensate wave function is then obtained by numerically integrating Eq. (4) with spatial resolutions $\Delta\tilde{x}=\Delta\tilde{y}=\Delta\tilde{z}=0.1$ and a time step of 10^{-3} using the fourth-order Runge-Kutta method [35] (see Supplemental Material [36]).

Simulation results.—The evolution of the quasi-2D BEC from a typical initiate state in both the disk geometry and the spherical shell geometry can be seen in the movies in the Supplemental Material [36]. In Fig. 2, we show snapshots of the condensate density on the $\tilde{z}=0$ plane for the disk BEC and on the $\tilde{r}=\tilde{R}$ surface for the spherical BEC shell. In the disk BEC, the like-signed vortices tend to form transient clusters that grow with time, which eventually lead to two counterrotating persistent OV clusters. The annihilation of the vortices essentially ceases upon the formation of the OV clusters. These observations agree nicely with those of Ref. [11].

In the spherical BEC shell, the vortex-pair annihilations result in a somewhat more rapid decay of the total vortex number $N(\tilde{t})$, as shown in Figs. 2(c) and 2(d). Note that in 2D BECs, two vortices annihilate essentially via a multi-vortex interaction process [37–40]. When a general n-vortex process controls the vortex decay, a scaling of $N(\tilde{t})\propto\tilde{t}^{-(1/n-1)}$ is expected [40]. At large $\tilde{t}$ but before the OV clusters form in the disk BEC, we find that $N(\tilde{t})$ can be fitted well using this scaling with $n=2.4$ for the disk BEC and $n=3$ for the spherical shell BEC. The $n=3$ scaling is likely generic for pair annihilations in boundaryless quasi-2D BECs (see Supplemental Material [36]). On the other hand, the $n=2.4$ scaling for the disk BEC indicates the presence of both two-vortex and three-vortex

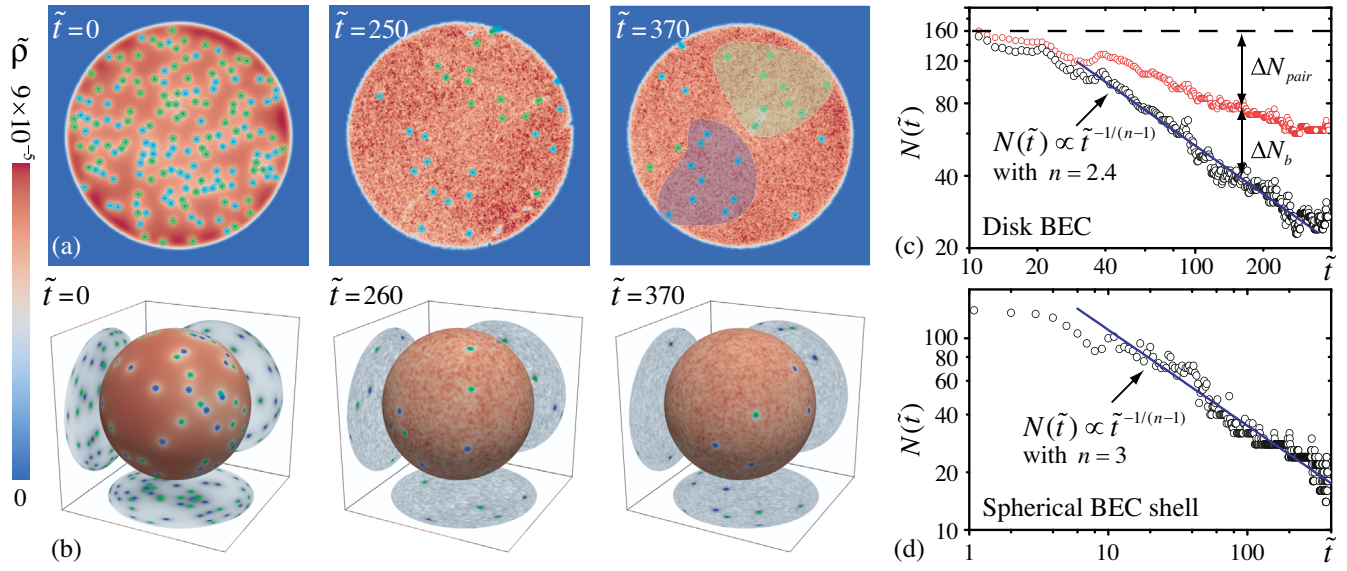

FIG. 2. (a),(b) The evolution of the condensate density $\tilde{\rho} = |\tilde{\psi}|^2$ in the Gross-Pitaevskii model for the quasi-2D BEC in the disk geometry and the spherical shell geometry, respectively. The vortices and antivortices are marked with dots of different colors for better visibility. The shaded regions in the disk BEC signify the places where coherent OV clusters are seen. (c),(d) The evolution of the total vortex number $N(\tilde{t})$ (black circles). The red circles in the disk BEC case give the partition of the decayed vortices due to the pair-annihilation process ΔN_{pair} and due to vortices exiting the boundaries ΔN_b.

processes. Indeed, there are two distinct processes through which the vortices can decay in the disk BEC, i.e., pair annihilations and exiting from the disk boundary. The exiting process may be regarded as the annihilation of a vortex with its image charge in the presence of a second vortex, i.e., essentially a two-vortex process. According to Fig. 2(c), about 1/3 of the decayed vortices in the disk BEC are caused by vortex exiting.

Despite the more rapid annihilation of the vortex pairs in the spherical BEC shell, there appear to be no vortex clusters at any time [see Fig. 2(b)]. More concrete evidence showing whether or not OV clusters ever form in a BEC can be obtained from the evolution of the vortex energy [41]. Note that the total kinetic energy of a BEC consists of three parts: an incompressible part due to the flow field induced by the vortices, a compressible part due to sound waves, and a quantum pressure term [42]. Many past studies evaluated the incompressible kinetic energy associated with the vortex system in planar BECs by first extracting the core locations of all vortices and then applying the following point-vortex Hamiltonian [11–13,15,16]:

$$\mathcal{H} = -\frac{\rho_0\kappa^2}{4\pi}\left[\sum_{i<j} s_i s_j \ln(|\mathbf{r}'_\mathbf{i} - \mathbf{r}'_\mathbf{j}|^2) - \sum_i s_i^2 \ln(1 - r_i'^2) - \sum_{i<j} s_i s_j \ln\left(1 - 2\mathbf{r}'_\mathbf{i}\cdot\mathbf{r}'_\mathbf{j} + |r'_i|^2|r'_j|^2\right)\right], \quad (5)$$

where ρ_0 is the mean density, $\kappa = h/m$ is the quantized circulation, and $\mathbf{r}'_\mathbf{i} = \mathbf{r}_\mathbf{i}/R$ denotes the normalized position vector of the ith vortex with a winding number $s_i = \pm 1$. Here we adopt the same procedures. For vortices in the spherical shell, the following Hamiltonian is used [43,44]:

$$\mathcal{H} = -\frac{\rho_0\kappa^2}{4\pi}\sum_{i<j} s_i s_j \ln(1 - \mathbf{r}'_\mathbf{i}\cdot\mathbf{r}'_\mathbf{j}). \quad (6)$$

The variations of the normalized incompressible kinetic energy $E_V = (4\pi/\rho_0\kappa^2)\mathcal{H}$ in both BEC geometries are calculated and shown in Fig. 3. For reference purposes, we have also included in Fig. 3 the threshold energy $E_c(N)$ above which a 2D neutral N-vortex system enters the negative temperature regime. This $E_c(N)$ is derived via a Markov chain Monte-Carlo method [45] using the above Hamiltonians (see Supplemental Material [36]). Since OV clusters appear only at energies significantly higher than $E_c(N)$ [13], we also introduce a reference energy $E^*(N)$ at which the mean dipole (or quadrupole) moment of the vortices equals 30% of the value for the limiting configuration depicted in Fig. 1. Above $E^*(N)$, clear vortex clusters are readily observable. Both $E_c(N)$ and $E^*(N)$ vary with $\tilde{t}$ as the total vortex number $N(\tilde{t})$ decays. From Fig. 3, one can see that for the disk BEC the vortex energy E_V quickly rises to above $E^*(N)$, which explains why OV clusters were observed. On the contrary, E_V for the spherical BEC shell barely gets above $E_c(N)$ and is always below $E^*(N)$, which thereby confirms that OV clusters never formed in the spherical BEC shell.

The contrasting fate of the vortices in the disk BEC and the spherical BEC shell calls for an explanation. As we discussed earlier, the vortices in the spherical BEC shell can decay only via pair annihilations, whereas in the disk BEC

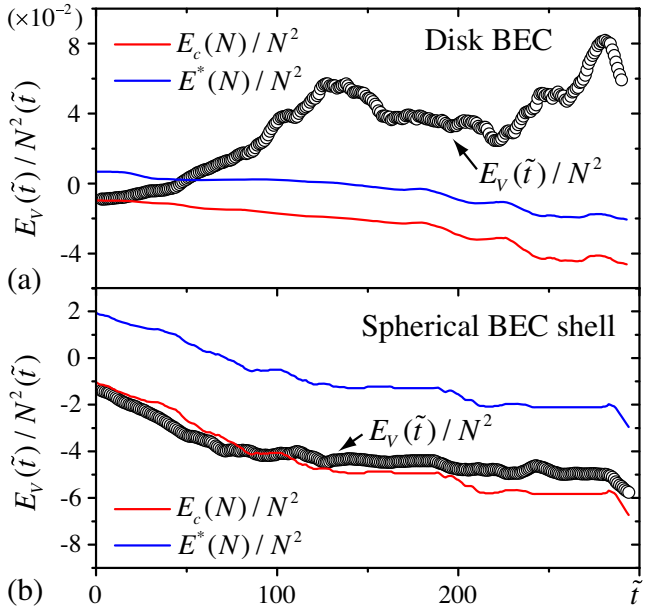

FIG. 3. Evolution of the incompressible kinetic energy E_V associated with the vortices in (a) the disk BEC and (b) the spherical BEC shell. $E_c(N)$ is the threshold energy for transition to the negative temperature state, and $E^*(N)$ is a reference energy above which vortex clusters are readily observable.

they can decay via both pair annihilations and exiting from the boundary. To better understand the consequence of this difference, we simulated the annihilation of an isolated vortex pair and the exiting of a single vortex in the disk BEC using GPE. For the annihilation test, we first prepare a vortex-antivortex pair at close separation and then evolve Eq. (4) with a small added damping so the two vortices approach each other while the pair propagates [40]. When the vortex separation is about the core size, we set $\tilde{t} = 0$ and remove the added damping, so the subsequent annihilation process is not affected by artificial dissipation. Similar procedures are adopted for the single vortex near the disk boundary. The results are shown in Fig. 4. One can see that

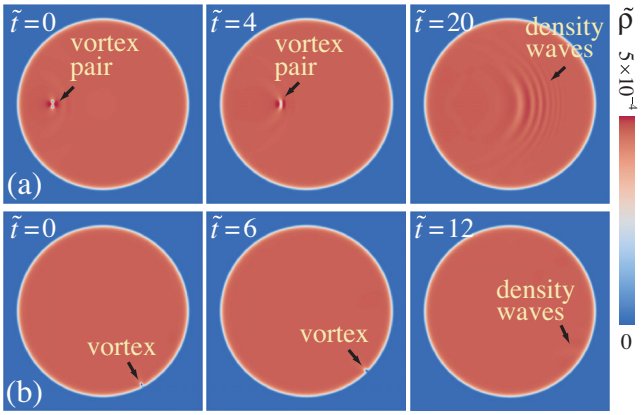

FIG. 4. GPE simulation showing density variations in the disk BEC when (a) a vortex-antivortex pair undergoes annihilation and (b) a vortex merges into the disk boundary.

the pair annihilation in bulk BEC generates intense sound waves due to the conservation of linear momentum. On the contrary, in the vortex-exiting process, the vortex merges into the zero-density region, which hardly generates any sound waves.

The sound waves in the BECs can damp out the vortex motion and dissipate the incompressible kinetic energy possessed by the vortex system [37]. This process is similar in nature to the mutual friction damping on quantized vortices in superfluid helium caused by the normal-fluid component [46–48]. Therefore, one may draw the following conclusions: i) the pair-annihilation process alone does not lead to the formation of OV clusters due to the intense sound emission and ii) the exiting of the vortices from the BEC boundaries, which increases the mean energy of the vortices with minimal sound emission, is the true mechanism responsible for spontaneous vortex orders. To verify these conclusions, we present two complementary tests that can produce unequivocal supporting evidence.

Complementary tests.—In the first test, we examine the ideal dynamics of the vortices on the spherical surface ($\tilde{R} = 15$) without sound waves. To do this, we consider point vortices with the same initial distribution as in our GPE simulation and evolve them using the equation of motion derived from the Hamiltonian in Eq. (6) [43,44]:

$$\frac{d\mathbf{r}_i'}{d\tilde{t}} = \frac{1}{2\tilde{R}^2}\sum_{j\neq i}\frac{\mathbf{r}_j' \times \mathbf{r}_i'}{1-\mathbf{r}_j'\cdot\mathbf{r}_i'}. \tag{7}$$

To mimic the vortex-pair annihilation process, we remove vortex-antivortex pairs whenever the arc-length separation between two vortices is less than $0.03\tilde{R}$ [11]. At large $\tilde{t}$, we find that four vortex clusters form spontaneously as shown in Fig. 5, which eventually evolve toward the limiting configuration given in Fig. 1(b). This dynamic is not surprising, because removing a vortex pair at close separation essentially amounts to subtracting a large negative quantity from the Hamiltonian. Therefore, the energy of the point-vortex system steadily increases with time, which inevitably leads to the formation of OV clusters. The exact time it takes before OV clusters emerge depends on the

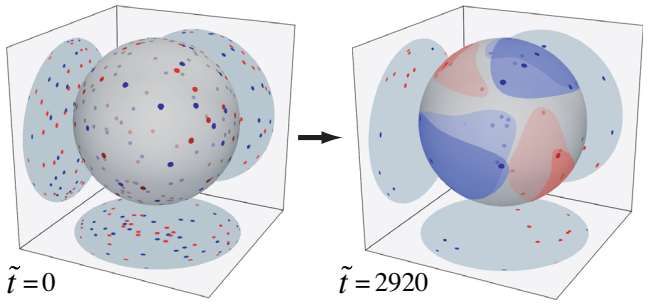

FIG. 5. Point-vortex model simulation of the vortex dynamics on a 2D spherical surface from the same initial state as in our GPE simulation.

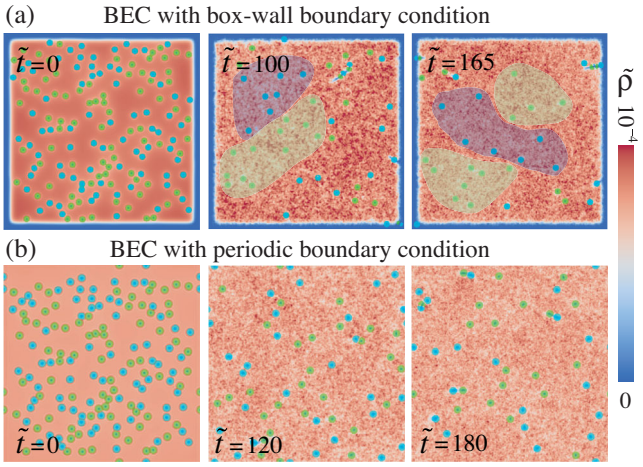

FIG. 6. GPE simulation of the vortex dynamics in quasi-2D square BEC with (a) box-wall boundary condition and (b) periodic boundary condition.

threshold separation for vortex-pair removal. This test shows that the evaporative-heating mechanism would work only in the absence of sound waves. Our result also calls for caution when using the point-vortex model to understand the vortex dynamics in real BECs.

In the second test, we conduct a GPE simulation with 80 vortices and 80 antivortices at random locations in a square-shaped planar quasi-2D BEC. We adopt the same trapping parameters U_0 and ω as for the disk BEC and set the side length of the square to $\tilde{R} = 50$ so its area is also similar. We can now apply either the box-wall boundaries (i.e., with the hyperbolic tangent potential) or the periodic boundaries [40] so that the vortex dynamics in the same BEC geometry with and without the vortex-exiting mechanism can be compared directly. Figure 6 shows representative snapshots of the BEC density from the same initial state with the two boundary conditions. Large-scale OV clusters are seen only in the case with the box-wall boundaries. We have also tested the vortex evolution in a curved BEC with a boundary for vortex exiting (i.e., a quasi-2D spherical BEC cap) and again observed OV clusters (see Supplemental Material [36]). These results unambiguously demonstrate the crucial role of the vortex-exiting boundaries in the spontaneous formation of vortex orders.

In summary, we have examined the evolution of vortices in both planar and spherical 2D BECs. A comprehensive understanding of the mechanism underlying the spontaneous vortex orders is achieved, which represents major progress in the study of the far-from-equilibrium dynamics of 2D superfluids. Our findings may also motivate future experiments in 2D spherical BECs at the International Space Station.

The authors thank S. Nazarenko and K. Helmerson for stimulating discussions. The authors also acknowledge support by the National Science Foundation under Grant No. DMR-2100790. The work was conducted at the National High Magnetic Field Laboratory, which is supported by National Science Foundation Cooperative Agreement No. DMR-1644779 and the state of Florida.

*Corresponding author.
wguo@magnet.fsu.edu

[1] H. Kellay and W. I. Goldburg, Two-dimensional turbulence: A review of some recent experiments, Rep. Prog. Phys. **65**, 845 (2002).
[2] A. Adriani, A. Mura, G. Orton *et al.*, Clusters of cyclones encircling jupiters poles, Nature (London) **555**, 216 (2018).
[3] L. Onsager, Statistical hydrodynamics, II Nuovo Cimento **6**, 279 (1949).
[4] G. L. Eyink and K. R. Sreenivasan, Onsager and the theory of hydrodynamic turbulence, Rev. Mod. Phys. **78**, 87 (2006).
[5] G. Boffetta and R. E. Ecke, Two-dimensional turbulence, Annu. Rev. Fluid Mech. **44**, 427 (2012).
[6] S. P. Johnstone, A. J. Groszek, P. T. Starkey, C. J. Billington, T. P. Simula, and K. Helmerson, Evolution of large-scale flow from turbulence in a two-dimensional superfluid, Science **364**, 1267 (2019).
[7] G. Gauthier, M. T. Reeves, X. Yu, A. S. Bradley, M. A. Baker, T. A. Bell, H. Rubinsztein-Dunlop, M. J. Davis, and T. W. Neely, Giant vortex clusters in a two-dimensional quantum fluid, Science **364**, 1264 (2019).
[8] Y. P. Sachkou, C. G. Baker, G. I. Harris, O. R. Stockdale, S. Forstner, M. T. Reeves, X. He, D. L. McAuslan, A. S. Bradley, M. J. Davis, and W. P. Bowen, Coherent vortex dynamics in a strongly interacting superfluid on a silicon chip, Science **366**, 1480 (2019).
[9] E. Varga, V. Vadakkumbatt, A. J. Shook, P. H. Kim, and J. P. Davis, Observation of Bistable Turbulence in Quasi-Two-Dimensional Superflow, Phys. Rev. Lett. **125**, 025301 (2020).
[10] R. J. Donnelly, *Quantized Vortices in Helium II* (Cambridge University Press, Cambridge, England, 1991).
[11] T. Simula, M. J. Davis, and K. Helmerson, Emergence of Order from Turbulence in an Isolated Planar Superfluid, Phys. Rev. Lett. **113**, 165302 (2014).
[12] T. P. Billam, M. T. Reeves, B. P. Anderson, and A. S. Bradley, Onsager-Kraichnan Condensation in Decaying Two-Dimensional Quantum Turbulence, Phys. Rev. Lett. **112**, 145301 (2014).
[13] X. Yu, T. P. Billam, J. Nian, M. T. Reeves, and A. S. Bradley, Theory of the vortex-clustering transition in a confined two-dimensional quantum fluid, Phys. Rev. A **94**, 023602 (2016).
[14] A. J. Groszek, T. P. Simula, D. M. Paganin, and K. Helmerson, Onsager vortex formation in bose-einstein condensates in two-dimensional power-law traps, Phys. Rev. A **93**, 043614 (2016).
[15] M. T. Reeves, T. P. Billam, X. Yu, and A. S. Bradley, Enstrophy Cascade in Decaying Two-Dimensional Quantum Turbulence, Phys. Rev. Lett. **119**, 184502 (2017).

[16] A. J. Groszek, M. J. Davis, D. M. Paganin, K. Helmerson, and T. P. Simula, Vortex Thermometry for Turbulent Two-Dimensional Fluids, Phys. Rev. Lett. **120**, 034504 (2018).
[17] R. Pakter and Y. Levin, Nonequilibrium Statistical Mechanics of Two-Dimensional Vortices, Phys. Rev. Lett. **121**, 020602 (2018).
[18] J. Han and M. Tsubota, Onsager vortex formation in two-component Bose-Einstein condensates, J. Phys. Soc. Jpn. **87**, 063601 (2018).
[19] D. Maestrini and H. Salman, Entropy of negative temperature states for a point vortex gas, J. Stat. Phys. **176**, 981 (2019).
[20] A. Tononi and L. Salasnich, Bose-Einstein Condensation on the Surface of a Sphere, Phys. Rev. Lett. **123**, 160403 (2019).
[21] A. Tononi, F. Cinti, and L. Salasnich, Quantum Bubbles in Microgravity, Phys. Rev. Lett. **125**, 010402 (2020).
[22] K. Padavić, K. Sun, C. Lannert, and S. Vishveshwara, Vortex-antivortex physics in shell-shaped Bose-Einstein condensates, Phys. Rev. A **102**, 043305 (2020).
[23] N. S. Móller, F. E. A. dos Santos, V. S. Bagnato, and A. Pelster, Bose-Einstein condensation on curved manifolds, New J. Phys. **22**, 063059 (2020).
[24] S. J. Bereta, M. A. Caracanhas, and A. L. Fetter, Superfluid vortex dynamics on a spherical film, Phys. Rev. A **103**, 053306 (2021).
[25] O. Zobay and B. M. Garraway, Two-Dimensional Atom Trapping in Field-Induced Adiabatic Potentials, Phys. Rev. Lett. **86**, 1195 (2001).
[26] Y. Colombe, E. Knyazchyan, O. Morizot, B. Mercier, V. Lorent, and H. Perrin, Ultracold atoms confined in rf-induced two-dimensional trapping potentials, Europhys. Lett. **67**, 593 (2004).
[27] T. L. Harte, E. Bentine, K. Luksch, A. J. Barker, D. Trypogeorgos, B. Yuen, and C. J. Foot, Ultracold atoms in multiple radio-frequency dressed adiabatic potentials, Phys. Rev. A **97**, 013616 (2018).
[28] E. R. Elliott, M. C. Krutzik, J. R. Williams, R. J. Thompson, and D. C. Aveline, NASA's Cold Atom Lab (CAL): System development and ground test status, npj Microgravity **4**, 16 (2018).
[29] N. Lundblad, R. A. Carollo, C. Lannert, M. J. Gold, X. Jiang, D. Paseltiner, N. Sergay, and D. C. Aveline, Shell potentials for microgravity Bose-Einstein condensates, npj Microgravity **5**, 30 (2019).
[30] L. P. Pitaevskii and S. Stringari, *Bose-Einstein Condensation* (Oxford University Press, Oxford, 2003).
[31] T. W. Neely, A. S. Bradley, E. C. Samson, S. J. Rooney, E. M. Wright, K. J. H. Law, R. Carretero-González, P. G. Kevrekidis, M. J. Davis, and B. P. Anderson, Characteristics of Two-Dimensional Quantum Turbulence in a Compressible Superfluid, Phys. Rev. Lett. **111**, 235301 (2013).
[32] T. Kanai, W. Guo, and M. Tsubota, Flows with fractional quantum circulation in Bose-Einstein condensates induced by nontopological phase defects, Phys. Rev. A **97**, 013612 (2018).
[33] T. Kanai, W. Guo, M. Tsubota, and D. Jin, Torque and Angular-Momentum Transfer in Merging Rotating Bose-Einstein Condensates, Phys. Rev. Lett. **124**, 105302 (2020).
[34] M. L. Chiofalo, S. Succi, and M. P. Tosi, Ground state of trapped interacting Bose-Einstein condensates by an explicit imaginary-time algorithm, Phys. Rev. E **62**, 7438 (2000).
[35] W. H. Press, B. P. Flannery, S. A. Teukolsky, and W. T. Vetterling, *Numerical Recipes in C. The Art of Scientific Computing* (Cambridge University Press, Cambridge, England, 1992).
[36] See Supplemental Material at http://link.aps.org/supplemental/10.1103/PhysRevLett.127.095301 for movies and further discussions of the Gross-Pitaevskii and point-vortex model simulations.
[37] S. Nazarenko and M. Onorato, Freely decaying turbulence and Bose-Einstein condensation in Gross-Pitaevski model, J. Low Temp. Phys. **146**, 31 (2007).
[38] W. Jin Kwon, G. Moon, J.-y. Choi, S. Won Seo, and Y.-i. Shin, Relaxation of superfluid turbulence in highly oblate Bose-Einstein condensates, Phys. Rev. A **90**, 063627 (2014).
[39] A. Cidrim, F. E. A. dos Santos, L. Galantucci, V. S. Bagnato, and C. F. Barenghi, Controlled polarization of two-dimensional quantum turbulence in atomic Bose-Einstein condensates, Phys. Rev. A **93**, 033651 (2016).
[40] A. W. Baggaley and C. F. Barenghi, Decay of homogeneous two-dimensional quantum turbulence, Phys. Rev. A **97**, 033601 (2018).
[41] R. H. Kraichnan and D. Montgomery, Two-dimensional turbulence, Rep. Prog. Phys. **43**, 547 (1980).
[42] C. J. Pethick and H. Smith, *Bose-Einstein Condensation in Dilute Gases* (Cambridge University Press, Cambridge, England, 2008).
[43] V. A. Bogomolov, Dynamics of vorticity at a sphere, Fluid Dyn. **12**, 863 (1977).
[44] D. G. Dritschel, M. Lucia, and A. C. Poje, Ergodicity and spectral cascades in point vortex flows on the sphere, Phys. Rev. E **91**, 063014 (2015).
[45] J. A. Viecelli, Equilibrium properties of the condensed states of a turbulent two-dimensional neutral vortex system, Phys. Fluids **7**, 1402 (1995).
[46] J. Gao, W. Guo, and W. F. Vinen, Determination of the effective kinematic viscosity for the decay of quasiclassical turbulence in superfluid ^{4}He, Phys. Rev. B **94**, 094502 (2016).
[47] J. Gao, W. Guo, S. Yui, M. Tsubota, and W. F. Vinen, Dissipation in quantum turbulence in superfluid ^{4}He above 1 K, Phys. Rev. B **97**, 184518 (2018).
[48] S. Yui, H. Kobayashi, M. Tsubota, and W. Guo, Fully Coupled Two-Fluid Dynamics in Superfluid ^{4}He: Anomalous Anisotropic Velocity Fluctuations in Counterflow, Phys. Rev. Lett. **124**, 155301 (2020).